- Investigation of the use of two detectors mounted at different heights for vehicle radiation surveys.
- Ambient dose equivalent rates from dual-detector setup were closer to reference measurements than from single detectors.
- Radiocesium scrubbing from asphalt means ambient dose equivalent rates above roads are not necessarily representative of rates adjacent to roads.
- Ratio of results from two detectors indicates whether radiocesium is deficient on roads compared to adjacent land.

Using two detectors concurrently to monitor ambient dose equivalent rates in vehicle surveys of radiocesium contaminated land

Minoru Takeishi[1*], Masaru Shibamichi[2], Alex Malins[3], Hiroshi Kurikami[4], Mitsuhiro Murakami[5], Jun Saegusa[6], Masayuki Yoneya[7]

[1*]Japan Atomic Energy Agency (JAEA), Fukushima Environmental Safety Center, 10-2 Fukasaku, Miharu-machi, Tamura-gun, Fukushima 963-7700, Japan, takeishi.minoru@jaea.go.jp, Tel: +81-247-61-2910

[2]Japan Atomic Energy Agency (JAEA), Fukushima Environmental Safety Center, 10-2 Fukasaku, Miharu-machi, Tamura-gun, Fukushima 963-7700, Japan, shibamichi.masaru@jaea.go.jp

[3]Japan Atomic Energy Agency (JAEA), Center for Computational Science and e-Systems, 178-4-4 Wakashiba, Kashiwa, Chiba 277-0871, Japan, malins.alex@jaea.go.jp

[4]Japan Atomic Energy Agency (JAEA), Fukushima Environmental Safety Center, 10-2 Fukasaku, Miharu-machi, Tamura-gun, Fukushima 963-7700, Japan, kurikami.hiroshi@jaea.go.jp

[5]Inspection Development Company Ltd (IDC), 3129-37 Hirahara, Muramatsu, Tokai-mura, Ibaraki 319-1112, Japan, murakami.mitsuhiro@jaea.go.jp

[6]Japan Atomic Energy Agency (JAEA), Collaborative Laboratories for Advanced Decommissioning Science, 2-4 Shirakata, Tokai-mura, Ibaraki 319-1195, Japan, saegusa.jun@jaea.go.jp

[7]Japan Atomic Energy Agency (JAEA), Fukushima Environmental Safety Center, Environmental Radiation Center, 45-169 Sukakeba, Kaibama, Haramachi-ku, Minamisoma-shi, Fukushima 975-0036, Japan, yoneya.masayuki@jaea.go.jp

*Corresponding author

Abstract

In response to the accident at Tokyo Electric Power Company's Fukushima Dai-ichi Nuclear Power Plant (FDNPP), vehicle-borne monitoring was used to map radiation levels for radiological protection of the public. By convention measurements from vehicle-borne surveys are converted to the ambient dose equivalent rate at 1 m height in the absence of the vehicle. This allows for comparison with results from other types of survey, including surveys with hand-held or airborne instruments. To improve the accuracy of the converted results from vehicle-borne surveys, we investigated combining measurements from two detectors mounted on the vehicle at different heights above the ground. A dual-detector setup was added to a JAEA monitoring car and compared against hand-held survey meter measurements in Fukushima Prefecture. The results obtained by combining measurements from two detectors were within ±20% of the hand-held reference measurements. The mean absolute percentage deviation from the reference measurements was 7.2%. The combined results from the two detectors were more accurate than those from either the roof-mounted detector, or the detector inside the vehicle, taken alone. One issue with vehicle-borne surveys is that ambient dose equivalent rates above roads are not necessarily representative of adjacent areas. This is because radiocesium is often deficient on asphalt surfaces, as it is easily scrubbed off by rain, wind and vehicle tires. To tackle this issue, we investigated mounting heights for vehicle-borne detectors using Monte Carlo gamma-ray simulations. When radiocesium is deficient on a road compared to the adjacent land, mounting detectors high on vehicles yields results closer to the values adjacent to the road. The ratio of ambient does equivalent rates reported by detectors mounted at different heights in a dual-detector setup indicates whether radiocesium is deficient on the road compared to the adjacent land.

Keywords:

Vehicle-borne survey; dual-detector monitoring; dose rate conversion; Fukushima Dai-ichi Nuclear Power Plant; radiation monitoring

1. Introduction

In the emergency response to the accident of Tokyo Electric Power Company (TEPCO) Fukushima Dai-ichi Nuclear Power Plant (FDNPP) in March 2011 (hereafter, the FDNPP accident), the headquarters against nuclear disasters in the Japanese Government enacted various measures for radiological protection of the public. One component was the production of dose rate maps (DRM) and accumulated dose estimation maps (ADEM) by combining various measurements of dose rates in the field and interpolating between the spatially discrete data points (Headquarters against Nuclear Disasters, 2011; MEXT, 2011a).

Field monitoring results were uploaded to the website of the Ministry of Education, Culture, Sports, Science and Technology (MEXT) from March 2011, succeeded by the Nuclear Regulation Authority (NRA) from September 2012 (MEXT and NRA, 2012). Evaluated DRM and ADEM were updated monthly with the latest measurements and published on the NRA website (MEXT, 2011b). JAEA cooperated in creating the DRM and ADEM. The maps incorporate the results of many kinds of dose rate measurement, including from hand-held survey meters, fixed monitoring posts (MP), vehicle-borne monitoring (VBM), and accumulated doses from electronic pocket dosimeters (EPD) (MEXT, 2011b). To combine the data and produce the dose rate contour maps, it was necessary to convert the measurements by various instruments into a single, comparable, quantity. By convention the ambient dose equivalent rate ($H^*(10)$ – μSv/h, International Commission on Radiological Protection (ICRP) 1996) at 1 m height, in the absence of detection apparatus, is used for this purpose.

In the early aftermath of the FDNPP accident, dedicated monitoring vehicles (DMV) deploying predominantly roof-mounted detectors were used to track and map releases from the FDNPP site (The Investigation Committee, 2011). Roof-mounted detectors are specifically designed for tracking radioactive plumes. On the other hand, aerial monitoring was superior in providing wide-area contamination measurements across Fukushima Prefecture and Japan. Methods to convert the airborne measurements to the ambient dose equivalent rate at 1 m height were developed specifically for Japan's natural environment, accounting for natural background radiation and factors such as forests and mountainous topography (Torii et. al., 2012; Sanada et. al., 2014, 2016; Sanada and Torii, 2015).

From August 2011 it became a priority to produce maps of the ambient dose equivalent rate at 1 m height with detailed spatial resolution to determine effective

doses from external radiation to the local population (Monitoring Coordination Meeting, 2016). VBM offers better spatial resolution than airborne monitoring, but also allows for faster coverage of contaminated areas than static measurement posts and person-borne monitoring surveys (IAEA, 2003).

The portable monitoring systems KURAMA (Kyoto University RAdiation MApping system) and KURAMA-II were developed by the Kyoto University Research Reactor Institute (KURRI) in the early aftermath of the FDNPP accident (Tanigaki et al., 2012, 2013; Tsuda et al., 2013, 2015). The main improvements of the KURAMA-II system over KURAMA are as follows. KURAMA-II is more compact and fully autonomous. KURAMA-II employs a higher efficiency CsI detector (Hamamatsu C12137 detector) instead of KURAMA's NaI detector. KURAMA-II also collects pulse-height spectra by using the CompactRIO platform from National Instruments. Both KURAMA and KURAMA-II can be loaded into all vehicle types, including ordinary cars. The devices have been deployed for monitoring ambient dose equivalent rates across North-East Japan by the Japanese Government (Andoh et al., 2015).

Since 2012 the effective doses in Fukushima Prefecture has been mainly caused by external radiation from ^{134}Cs and ^{137}Cs deposited on the ground, so called groundshine radiation (MEXT and NRA, 2012; UNSCEAR, 2014; Katata et al. 2015). Kinase et al. (2015) reported that ambient dose equivalent rates above the center of paved roads in Kawamata, Fukushima Prefecture, were lower than adjacent areas. The measurements were highest at the edges of the roads where they met the surrounding environments. It was suggested that radiocesium deposited on the road was washed out by rain towards the verges and drainage channels.

The heterogeneous nature of ambient dose equivalent rates around roads raises the question of how to apply VBM results above roads for calculating annual effective doses (mSv/y) to the public. For Fukushima residents, annual effective doses are typically accrued inside homes, schools and offices (Naito et al., 2015; Nomura et al., 2016; Naito et al., 2016). For outdoor workers, such as farmers and workers in the decontamination, forestry and construction sectors, doses received outdoors away from roads are important. Doses received during transit are generally a relatively small component of the overall exposures. Research is needed on ways to extract results from vehicle-borne surveys that are representative of the main exposures received within homes and at workplaces.

JAEA operates a dedicated vehicle for monitoring radiation in the environment (hereafter referred to as the DMVj – Dedicated Monitoring Vehicle JAEA). In this study we installed an additional detector inside the DMVj vehicle to complement the original detector setup mounted on the roof. As the detectors were installed at different heights above the ground, they have different fields of view of the environmental radiation. The performance of the dual-detector setup versus using only one detector was checked at calibration sites in Fukushima Prefecture. We deployed the dual-detector setup at various locations within the evacuated zone surrounding FDNPP to understand how its measurements are affected by factors such as land use, topography and decontamination. We checked the effect of passenger number and fuel level on the DMVj monitoring results. Finally, we performed a Monte Carlo radiation transport calculation for ambient dose equivalent rates above roads in the absence of detection equipment. The results show how height and distance from the center of the road affect $H^*(10)$.

2. Methods

2.1 Instruments

The specifications of the monitoring vehicle used in this study are shown in Fig. 1. A NaI(Tl) scintillation detector (Hitachi ADP-1122) is installed on top of the DMVj at approximately 2 m height above the ground. The detector measures the absorbed dose rate in air (D_e – μGy/h) over the range 0.01-10 μGy/h for photons in the energy range 50 keV to 3 MeV. The energy resolution is within 10% at 662 keV (^{137}Cs photopeak). The Hitachi ADP-1122 employs a 2”ϕ x 2” NaI(Tl) crystal. Due to the large crystal size this detector has higher sensitivity than typical hand-held survey meters, such as the Hitachi TCS-172B. The detector was calibrated using a ^{137}Cs radiation source, certified as 10 MBq on 2nd May 2013 by the Japan Calibration Service System (JCSS). The source was fixed at 1 m above the detector. The detector was calibrated against the (decay-corrected) absorbed dose rate in air at 1 m distance from the source specified on the JCSS calibration sheet. The drift of the detector reading is checked yearly and the detector is recalibrated if the result is more than ±10% from the reference value.

The low range Hitachi ADP-1122 detector is complimented by a silicon semiconductor detector (SSD, Hitachi ADP-225) mounted at the same height on the DMVj roof. The SSD detector covers a higher absorbed dose rate range (0.01-100 mGy/h), for photons with energy greater than 50 keV. The high range detector was calibrated with the JCSS ^{137}Cs source fixed at 20 cm above the detector. The drift is

checked yearly and recalibration is undertaken if the reading is more than ±20% from the reference result. Both the low and high range detectors are connected to a Hitachi ASM-1617 processing unit, which performs analog-to-digital conversion and energy compensation.

The external detectors on the DMVj were placed on the roof by design to give a wide field of view for measurement of cloud shine gamma-rays from radioactive plumes. The DMVj was repurposed in this study for the measurement of radiocesium ground-shine radiation in the Fukushima fallout contaminated area. A benefit of the placement of detectors on the vehicle roof is that it gives a wider field of view of ground-shine gamma-rays than detectors mounted close to 1 m height (Malins et al., 2015a).

To take measurements with a different field of view, an additional detector (Hitachi TCS-172B, 1”ϕ x 1” NaI(Tl) scintillator) was added inside the vehicle behind the passenger front seat, at approximately 0.9 m height above the ground. The signal of this detector is wired to a PC (Panasonic Toughbook CF-31 JEGAKDJ, Windows 7) via a digital recorder (Yokogawa Model DX1000). The detector measures ambient dose equivalent rate (H*(10) – ICRP 1996), denoted as H_i (μSv/h) for this detector’s measurements, over the range 0.01–30 μSv/h. The detector is sensitive to photons in the energy range 50 keV to 3 MeV.

The mounting position of the internal DMVj detector was decided so as to be as close to the 1 m reference height for environmental H*(10) measurements as possible. The mounting position was also chosen trying to minimize shielding by the vehicle engine, passengers and other detection apparatus carried onboard.

A second, identical, Hitachi TSC-172B unit was used in the person-borne hand-held survey measurements taken to provide a reference set for the DMVj results. Ambient dose equivalent rates were measured at 1 and 2 m height in the absence of the DMVj, denoted H_1 and H_2 (μSv/h), respectively. Both TSC-172B units were calibrated yearly using known radiation sources at the Facility of Radiation Standards at the Nuclear Science Research Institute in JAEA, in accordance with national standards from the National Metrology Institute of Japan (NMIJ of AIST).

The DMVj is also equipped with a sampler for radioactive dust and iodine monitoring instruments for use in nuclear emergencies (rear of vehicle, Fig. 1). This equipment was carried but not used during this study.

2.2 Conversion of vehicle-borne measurements

We studied the following procedures to convert the DMVj-borne measurements (D_e and H_i) to the ambient dose equivalent rate at 1 m height in the absence of the vehicle. The conversion procedures correct for the effects of shielding by the vehicle and its contents, and differences in height between the detector mounting positions and the 1 m reference height. In the case of the external rooftop detector measurements (D_e), the procedures also convert from absorbed dose rate in air (μGy/h) to ambient dose equivalent rate ($H^*(10)$ – μSv/h). The conversion procedures involve determining pairs of conversion coefficients *a priori* by correlating DMVj measurements at a set of calibration sites to reference measurements taken at the sites with the hand-held survey instrument.

The following equation was used to convert the measurements with the roof-mounted external detectors (D_e):

$$H_{1e} = a_{1e}D_e + b_{1e} \quad (1)$$

Here H_{1e} (μSv/h) corresponds to the ambient dose equivalent at 1 m height in the absence of the vehicle estimated from the external rooftop detector system. a_{1e} (μSv/h per μGy/h) and b_{1e} (μSv/h) are conversion coefficients obtained by linear regression of H_1 and D_e measurements over a set of calibration sites.

The DMVj internal detector measurements were converted using a corresponding formula:

$$H_{1i} = a_{1i}H_i + b_{1i} \quad (2)$$

Here H_{1i} (μSv/h) represents the ambient dose equivalent at 1 m height in the absence of the DMVj estimated from the internal detector measurement. The conversion coefficients, a_{1i} (dimensionless) and b_{1i} (μSv/h), are obtained by a linear least squares regression of H_1 and H_i from the calibration sites.

To employ both DMVj external and internal detector measurements concurrently in a dual-detector setup, we took a weighted average of H_i and D_e to estimate the ambient dose equivalent rate at 1 m height in the absence of the vehicle (denoted H_{1d}):

$$H_{1d} = a_{1d}H_i + b_{1d}D_e \quad (3)$$

To obtain the weights a_{1d} (dimensionless) and b_{1d} (μSv/h per μGy/h), we performed a linear regression of H_1/D_e against H_i/D_e using the data from the calibration sites.

We also checked the performance of the external, internal and dual-detector systems for estimating the ambient dose equivalent rate at 2 m height, in the absence of the vehicle. Corresponding formulae for H_{2e}, H_{2i} and H_{2d} followed from equations (1) to (3) and separate sets of conversion coefficients were derived using the H_2 reference measurements at the calibration sites. Table 1 summarizes the symbols and units of the various quantities in this paper.

Using hand-held reference measurements at field calibration sites to convert the DMVj measurements mirrors the conversion method for airborne surveys in Fukushima Prefecture (Sanada et al., 2014). One disadvantage of this method is the calibration sites have mixed radiation fields including terrestrial background, cosmic and radiocesium radiation. The relative intensity of these components varies between the calibration sites, while the radiocesium component can vary significantly on the scale of a few metres at a single calibration site. Another option is to calibrate the DMVj with detectors installed against known radiation sources (e.g. Buchanan et al., 2016), such as the JCSS 10 MBq ^{137}Cs source. However an advantage of calibrating with in situ radiation fields is that the radiation spectrum is closer to the radiation fields experienced operationally than for calibration with known radiation sources.

2.3 Details of calibration sites, reference measurements and subsequent field measurements

Measurements were taken at 29 calibration sites in the region surrounding FDNPP between March 2015 and February 2016. The DMVj was either parked on a paved road (R), on the side of a road (SR), in a paved parking lot (PL), or in a paved stopping space outside a building (SS). Furthermore two measurements were taken at bare land sites without surface asphalt (BL) for comparative purposes. The bare land sites were excluded from the fitting process to obtain the conversion coefficients for Equations (1) to (3), as vehicle-borne radiation surveys are mainly performed on the road network in Japan.

D_e and H_i were measured at each calibration site as follows. First the DMVj was stopped for more than 30 s to allow the detector count rates to saturate. Then five separate measurements were taken, each lasting 10 s. Reported D_e and H_i values are the mean of the five measurements, and uncertainties are their standard deviation.

The reference measurements with the hand-held survey meter (H_1 and H_2) were all taken after moving the DMVj vehicle more than 5 m away from the calibration site. H_1

measurements (i.e. at 1 m above the surface) were taken at all 29 calibration sites, while H_2 was measured at 24 of the locations. In a similar manner to the DMVj measurements, the hand-held survey meter count rate was allowed to saturate for more than 30 s at each calibration site prior to recording measurements. Five separate measurements lasting 10 s each were performed. The detection tube was held horizontally and rotated around between the measurements to point in five different directions, i.e. the measurement directions traced out the vertices of a pentagon. The reported H_1 and H_2 values are the mean of the measurements over five directions, and the reported uncertainty values are their standard deviation. The height of the hand-held instrument was calibrated against fixed length poles. A shorter pole with a mark at 1 m height was used for H_1 measurements, while a longer pole with clamp at 2 m height to hold the detector was used for H_2 measurements. The results of all the measurements at the calibration sites are listed in Table 2.

To test the dual-detector setup with a moving vehicle, we took a series of measurements driving through Fukushima Prefecture on February 9, 2016. The measurements covered both urban areas (including Fukushima City and Okuma Town), residential areas surrounded by forests, and other rural areas. The various land uses included both decontaminated and yet-to-be decontaminated sites. The DMVj speed was generally between 40 and 60 km/h when taking measurements. D_e was measured over 10 s intervals while the vehicle was moving. H_i was measured over 2 s intervals, so we report the mean of five consecutive measurements covering the same time period as the D_e measurements.

Three data points were available for H_1 without the DMVj present to check the moving DMVj measurements. The H_1 results were from a survey with the hand-held instrument conducted on April 16, 2015. The three results were decay corrected to February 9, 2016 for comparison with the DMVj measurements.

2.4 Measurements to check the effect of vehicle occupant number and fuel level

Buchanan et al. (2016) highlighted that vehicle fuel level and number of occupants could present time-varying sources of shielding for radiation detection equipment in vehicle-borne surveys. To check the size of these effects, on 17th March 2017 we measured D_e and H_i at four test sites with varying occupant number (0-3 occupants) and fuel level. The extent to which we could check the fuel-level dependency was limited by an operational rule requiring that the DMVj's 90 L fuel tank is always be more than

50% full so as to be ready in the event of a nuclear emergency. However, we checked the dependency of the results on fuel level both with a full tank and after a 135 km drive that burned around one-quarter of the initial fuel load.

2.5 Monte Carlo simulation

A Monte Carlo radiation transport simulation was performed to calculate how ambient dose equivalent rates vary across roads and adjacent land as a function of height above the surface. The simulation was executed with the Particle and Heavy Ion Transport code System (PHITS – Sato et al., 2013), ver. 2.82. We modeled a strip of road, 5 m wide, and effectively infinite in length (Fig. 2). The road material was asphalt, density 2.58 g/cm^3 (McConn Jr et al., 2011). Strips of flat ground, soil type, flanked the road on either side. A layer of air tops the model above. The densities and material compositions of soil and air followed Eckerman and Ryman (1993).

Cesium-134 and ^{137}Cs fallout was assumed to be distributed exponentially with depth within the soil and asphalt. The relaxation mass per area of the exponential distribution was 3.0 and 0.1 g/cm^2 for the soil and asphalt, respectively. The radiocesium activity per unit area of the asphalt surface was assumed to be 10 times lower than the soil, due to the scrubbing of radiocesium from the road surface by rainfall, wind and vehicle tires. Ambient dose equivalent rates ($H^*(10)$) were calculated at 0.5, 1, 2 and 3 m heights, as a function of perpendicular distance from the center of the road. The Monte Carlo relative uncertainties of the calculated $H^*(10)$ values were always less than 0.5%.

The simulations did not model the DMVj vehicle instruments, the hand-held survey meter or any of the associated detection apparatus explicitly. The results most closely represent the results that would be obtained in person-borne surveys using hand-held detectors or from fixed monitoring posts (e.g. the H_1 and H_2 reference measurements described above), as these survey methods convey lesser amounts of self-shielding than vehicle surveys.

3. Results and Discussion

3.1 Characteristics of ambient dose equivalent rates at the calibration sites

The ambient dose equivalent rates at the calibration sites varied from 0.12 to 22.6 μSv/h, as measured at 1 m height with the hand-held survey meter (Table 2). This

range covers levels from twice natural background radiation levels to some of the highest environmental radiation levels outside of the FDNPP site at the time of measurements.

The ambient dose equivalent rates at 1 and 2 m height (H_1 and H_2) were measured at 24 of the sites. At 17 of these locations, the ambient dose equivalent rate at 2 m height was higher than that at 1 m height. Figure 3 shows the ratio H_2/H_1 plotted against ascending H_1. The ratio H_2/H_1 does not depend on the magnitude of H_1.

The highest value of H_2/H_1 was 1.34, observed over a paved road approximately 5 m wide lying 0.5 km south of the FDNPP site boundary. The high number of locations with an ambient dose equivalent rate at 2 m height which is greater than at 1 m height is consistent with radiocesium having been scrubbed from the paved surfaces. The field of view of measurements taken near the ground is narrower than measurements taken at higher positions (Malins et al., 2015a). Therefore, if radiocesium has been scrubbed from an asphalt surface, this can give rise to the effect where the ambient dose equivalent rate at 2 m height is greater than that at 1 m height.

Although there are only data for two unpaved sites, the ratios H_2/H_1 for these sites are at the lower extremity of the results in Fig. 3. The second of these sites, ID O-5 (Table 2), lies close to the FDNPP site and presented the highest radiation levels. The bare land, measuring around 20 x 40 m, is surrounded on all sides by roads and buildings. The fact that H_2/H_1 is low at this site is consistent with radiocesium having been scrubbed from the surrounding asphalt and buildings. Due to a narrower field of view, the lower measurement (H_1) would have had a greater response to the radiocesium inventory on the bare land than the higher measurement (H_2), thus giving rise to the low H_2/H_1 ratio. This effect is exasperated in the DMVj monitoring results due to shielding of the external rooftop detectors from the bare land by the vehicle. The ratio D_e/H_i for this site was amongst the lowest observed.

To confirm that scrubbing had indeed occurred from asphalt surfaces, we measured the distribution of ambient dose equivalent rates in detail across the road at calibration site ID O-6 (H_2/H_1=1.34), which lies close to site O-5. H_1 increased with the distance from the center of the road (Fig. 4). H_1 was 8.82±0.38 μSv/h at the center of the road, rising to over 20 μSv/h on the grassland boarding the road. These results indicate that contamination levels on the verges are higher than on the road itself. The profiles of ambient dose equivalent rates across the road in Fig. 4 are similar to that of air kerma

rate above a road in Krasnae, Belarus, which was contaminated by Chernobyl accident fallout (Sakamoto and Saito, 2003).

3.2 Conversion of vehicle-borne monitoring results

The measurements from the external and internal vehicle detectors were converted to estimates for H_1 using Eqs. (1) and (2). Fig. 5 shows H_1 plotted against D_e (Fig. 5(a)) and H_i (Fig. 5(b)). The least squares method was used to determine coefficients a_{1e}, b_{1e}, a_{1i} and b_{1i}. The conversion parameters a_{1e} and b_{1e} correct the measurement D_e for the offset in height of the rooftop detector and the 1 m reference height, shielding by the DMVj vehicle, and conversion of units from μGy/h to μSv/h. By contrast, the primary correction by a_{1i} and b_{1i} to the internal measurement H_i is for vehicle shielding effects, given the smaller offset between the detector mounting and reference heights.

Both D_e and H_i were highly correlated with H_1, and the regression lines gave very good approximations of H_1 over the entire range of radiation levels. There is little scatter about the regression lines and the coefficient of determination (R^2) is greater than 0.98 in both cases. However, it is noteworthy that relative deviation from the regression line was large for the external detector results when H_1 was under 2 μSv/h, as described in the next section.

The datum for unpaved site O-5, which was not included in the regression, shows the largest deviation from the least squares line in Fig. 5(a) (D_e = 10.0±0.029 μGy/h, H_1= 22.6±0.34 μSv/h). As discussed in the previous section, this result is attributable to a radiocesium distribution around the site which has different characteristics than the typical radiocesium distribution for the calibration sites. Conversely, there is less of a discrepancy between the datum for site O-5 in Fig. 5(b) and the least squares line. The smaller offset between the vehicle internal detector (mounted at ~0.9 m) and the 1 m reference height means the fields of view of the DMVj and hand-held reference measurement are more closely matched. The differences in the characteristic distribution of radiocesium around paved and unpaved surfaces means that unpaved sites are not appropriate for use as calibration sites for vehicle-borne surveys to be conducted predominantly on roads. This observation is especially relevant if there is a large discrepancy between the fields of view of the vehicle detector and the reference $H^*(10)$ at 1 m height, caused for instance by different detector mounting heights or shielding by apparatus.

In comparison to the scatter of the single detector results about the regression lines (Fig. 5), the results for the dual show a larger amount of variation from the regression line (Fig. 6). The coefficient of determination for the least squares fitting is 0.772. The scatter reflects in part statistical uncertainty of the radiation measurements. It is also likely that factors relating to the distribution of radioactivity around the calibration sites, and differences in characteristics of the internal and external detectors, such as mounting height, shielding by the DMVj, and energy response curves, contribute to the scatter about the regression line. The simple nature of calibration in this study means it is not possible to determine the relative importance of these postulated causes. Employing a more controlled calibration environment, where the radiation source type and detector positioning and shielding can be controlled in a systematic way (e.g. Buchanan et al., 2016), would be effective in terms of understanding these factors.

3.3 Comparison of the single and dual-detector results

The results of the converted ambient dose equivalent rates obtained from both detectors separately (H_{1e} and H_{1i}), and by combing both internal and external measurements (H_{1d}) are shown in Fig. 7. The estimates from the dual-detector setup are closest to the H_1 reference measurements. The mean absolute percentage deviation of the dual-detector results compared to H_1 is 7.2%. The corresponding statistics are 45.2% and 14.8% for the external and internal detectors, respectively. The dual-detector results were all within ±20% of the hand-held survey meter measurements. The relative difference between H_{1d} and H_1 does not depend on the absolute value of H_1 (Fig. 8).

In contrast, the results from the external and internal detectors operated alone show larger deviations from H_1, particularly at the sites with ambient dose equivalent rates below 2 μSv/h (Fig. 8). The results from the internal detector (H_{1i}) are closer to the reference measurements than the external detector (H_{1e}). This is likely due to the smaller vertical offset of the internal detector from to the 1 m reference height than for the external detector.

To check whether the offset between the vehicle-borne detector height and the reference height was the main reason for the closer match between H_{1i} and H_1 than between H_{1e} and H_1, Fig. 9 shows the correlation of H_{2e} and H_{2i} with H_2. In this case the converted results from the external detector were closer to the reference measurements than the internal detector.

For the 2 m height case, again the dual-detector setup yielded results closest to the reference measurements compared to using the internal or external detector alone (Fig. 9(a)). H_{2d} were all within ±20% of the hand-held survey meter measurements (Fig. 9(b)). In the 2 m height case the weighting parameters for the dual-detector conversion procedure are a_{2d}=0.597 and b_{2d}=1.23, c.f. a_{1d}=0.909 and b_{1d}=0.758 for the 1 m height case (Fig. 6). The difference in the weights reflects a shift in the relative importance of the internal and external detector measurements in the 2 m height case. The external detector measurement (D_e) has a relatively higher contribution to the converted result at 2 m height than in the 1 m height case for the reasons of detector positioning and effective field of view.

3.4 Effects of occupant number and fuel level

Figure 10 shows the effects of occupant number and fuel level on the measured D_e and H_i at a four test sites. The test sizes covered from low to high ambient radiation levels. All measurements include the contribution of natural background radiation.

There was no clear dependency of the absorbed dose rates in air measured by the DMVj external detectors (D_e) on the number of occupants (Fig. 10(a) to (c)). The absorbed dose rates after consumption of fuel were slightly lower values than the values with a full fuel tank (Fig. 10(a)), although the decreases tended to be small (<0.01 μGy/h). This result is opposite to what would be expected if the fuel was a significant radiation shield, as the absorbed dose rates should then increase with decreasing fuel level.

Similar to the external detector case, the results for the internal detector showed no significant dependency on fuel level. The scatter of the results before and after the 135 km ride are within the statistical uncertainty (Fig. 10(d)).

No clear effect for numbers of occupants was seen on H_i when the ambient environmental radiation level was low (Fig. 10(d)). However for sites with higher ambient radiation levels, H_i decreased with increasing number of occupants (Fig. 10(e) and (f)). The internal detector is more sensitive to the shielding providing by occupants than the external detector due to its position between the forward and rear vehicle seats. The reason the shielding effect is not seen for the low dose rate sites (Fig. 10(a) and (d)) is likely related to low counting statistics giving high uncertainty, or the fact that the occupants themselves constitute a low intensity radiation source due to body ^{40}K content.

For the results of this paper outside this section, the DMVj was normally operated with one driver and two passengers, and the vehicle fuel level never dropped below 50%. Therefore we do not expect a significant impact of occupant number or fuel shielding on the other results presented.

3.5 Monte Carlo simulation of ambient dose equivalent rate distribution across road

The calculated ambient dose equivalent rate distribution across a model road via Monte Carlo simulation is shown in Fig. 11(a). The ambient dose equivalent rates are lowest above the center of the road for each height (0.5, 1, 2 and 3 m) above the surface. The ambient dose equivalent rates increase moving away from the center of the road towards the verges, where the radiocesium density is ten times higher per unit surface area than on the road.

The difference in ambient dose equivalent rates above the center of the road and away from the road is largest for the ambient dose equivalent rates at 0.5 m height (red line, diamond markers, Fig. 11(a)). The effect is less marked with increasing height above the ground surface (other lines, Fig. 11(a)). This is because the field of view of the radiocesium contributing to the ambient dose equivalent rate widens with increasing height above the ground (Malins et al., 2015a).

Mounting instrumentation higher on monitoring vehicles will yield more representative results for ambient dose equivalent rates away from roads, as the higher the mounting position the closer the ambient dose equivalent rate is to that at 1 m height furthest from the center of the road. If the purpose of the vehicle-borne radiation survey is to assess external radiation exposures to populations spending the majority of their time off roads, e.g. in homes, offices, and farmland, then higher mounting positions may be preferable.

The ratio of the ambient dose equivalent rate at 2 and 1 m height over the center of a road is related to the degree of radiocesium loss from the road compared to the adjacent land. The decontamination factor (DF) is defined as the ratio of the radiocesium activity per unit area away from the road compared to on the road. The data in Fig. 11(a) are for DF=10. Fig. 11(b) shows how H_2/H_1 varies as a function of DF. When no scrubbing from the road surface has occurred (DF=1), H_2/H_1=0.9. H_2/H_1 rises to a maximum of 1.3 when radiocesium is strongly deficient on the road surface compared to the adjacent land (high DF).

3.6 DMVj results during transit and effects of land use and heterogeneous radiocesium distributions

A demonstration of the dual-detector setup operated with a moving DMVj vehicle is shown in Fig. 12. The three reference measurements of H_1 with the hand-held survey meter along the course of the route lie close to the DMVj survey results. The closest matches are with the dual-detector results (H_{1d}) and the external detector operated alone (H_{1e}).

Figure 13 shows the ratio of the ambient dose equivalent rates measured at 2 and 1 m height by the dual-detector setup (H_{2d}/H_{1d}) as the vehicle was driven through areas with different land uses in Fukushima Prefecture. The land uses include decontaminated urban areas, where ambient dose equivalent rates were typically lower than 0.2 μSv/h, rural housing surrounded by trees, and forested mountains. Parts of the survey crossed the restricted zone close to the FDNPP site.

The ratio H_{2d}/H_{1d} tends to be high in areas that have not been decontaminated, such as forests (Fig. 13(c) and parts of (b)) and the restricted area (Fig. 13(d)). By contrast, the H_{2d}/H_{1d} ratio tends to be lower in decontaminated areas, such as Fukushima City (Fig. 13(a)) and areas where forests have been decontaminated to the first 20 m from roads (Fig. 13(b), circled area).

These results are attributed to difference in the radiocesium distribution. Non-decontaminated areas tend to have strong heterogeneity of the radiocesium distribution around roads, due to the scrubbing of radiocesium from the road surface. This gives rise to situations where the dose rate is higher at 2 m height than at 1 m height, as per Fig. 4.

On the roads through forests (Fig. 13(b) and (c)) there is also a possible topographic effect. The roads through forests tend to follow valley bottoms with forests rising up on either side. This geometry can rise to elevated radiation levels compared to if the ground were flat, with a larger effect at 2 m height than at 1 m height (Satoh et al., 2014; Malins et al., 2015b).

As the detectors are mounted at different heights, the ratio of measurements from the dual-detector system therefore provides information on the distribution of radiocesium around the measurement point. High H_{2d}/H_{1d} values indicates higher radiocesium activity levels adjacent to the road than on the road itself. This result offers the potential for correction schemes to be devised for measurements from vehicle-borne

radiation surveys, in order to generate more representative results for areas where residents predominantly spend time.

4. Conclusion

By installing an additional detector within a dedicated radiation survey monitoring vehicle, we were able to improve the accuracy of the converted ambient dose equivalent rates from vehicle-borne surveys. One benefits of the dual-detector setup is improved counting statistics. Another benefit if the detectors are mounted at different heights is two fields of view for the environmental radiation.

Mounting detectors higher on vehicles is appropriate if the purpose of the vehicle-borne radiation survey is to assess external exposure doses in the vicinity of living and working spaces adjacent to roads. This is because higher mounting positions are relatively more sensitive to radiation originating beyond the boundary of the road than lower mounting positions.

The ratio of the 2 to 1 m height ambient dose equivalent rates converted from the dual-detector setup (H_{2d}/H_{1d}) provides information on the heterogeneity of the radiocesium distribution around the road. A high ratio indicates that radiocesium activity levels on the road are lower than on the adjacent land.

Acknowledgments

The authors gratefully acknowledge the support of measurement as interns, Ryohei Shimomura (Kyoto University) and Yuta Endo (Toyohashi University of Technology). We also appreciate the advice offered by Kimiaki Saito (JAEA).

References

Andoh, M., Nakahara, Y., Tsuda, S., Yoshida, T., Matsuda, N., Takahashi, F., Mikami, S., Kinouchi, N., Sato, T., Tanigaki, M., Takamiya, K., Sato, N., Okumura, R., Uchihori, Y., Saito, K., 2015. Measurement of air dose rates over a wide area around the Fukushima Dai-ichi Nuclear Power Plant through a series of car-borne surveys. J. Environ. Radioact. 139, 266-280. DOI:10.1016/j.jenvrad.2014.05.014

Buchanan, E., Cresswell, A. J., Seitz, B., Sanderson, D. C. W., 2016. Operator related attenuation effects in radiometric surveys. Radiat. Meas. 86, 24-31. DOI: 10.1016/j.radmeas.2015.12.029

Eckerman, K.F., Ryman, J.C., 1993. External Exposure to Radionuclides in Air, Water, and Soil. Federal Guidance Report No. 12. U.S. Environmental Protection Agency. https://www.epa.gov/sites/production/files/2015-05/documents/402-r-93-081.pdf. (accessed 20.08.16)

Headquarters against Nuclear Disasters, Enforced Plan on Environmental Monitoring (April 22, 2011). http://radioactivity.nsr.go.jp/en/contents/1000/324/24/1304084_0422.pdf. (accessed 20.08.16)

International Atomic Energy Agency (IAEA), 2003. Guidelines for Radioelement Mapping using Gamma Ray Spectrometry Data, IAEA-TECDOC-1363, Vienna

International Commission on Radiological Protection (ICRP), 1996. Conversion coefficients for use in radiological Protection against external radiation. ICRP pub. 74 Ann. ICRP 26, 1-205. DOI:10.1016/ S0146-6453(96)90001-9

Investigation Committee on the Accident at the Fukushima Nuclear Power Stations of Tokyo Electric Power Company (The Investigation Committee), 2011. Interim Report; V. Emergency Response Measures Primarily Implemented outside the Fukushima Dai-ichi Nuclear Power Station in Response to the Accident, 281-425. http://www.cas.go.jp/jp/seisaku/icanps/eng/interim-report.html , (accessed 29.11. 16)

Katata, G., Chino, M., Kobayashi, T., Terada, H., Ota, M., Nagai, H., Kajino, M., Draxler, R., Hort, M. C., Malo, A., Torii, T., Sanada, Y., 2015. Detailed source term estimation of the atmospheric release for the Fukushima Daiichi Nuclear Power Station accident by coupling simulations of an atmospheric dispersion model with an improved deposition scheme and oceanic dispersion model. Atmos. Chem. Phys., 15, 1029-1070. DOI:10.5194/acp-15-1029-2015

Kinase, S., Sato, S., Sakamoto, R., Yamamoto, H., Saito, K., 2015. Changes in ambient dose equivalent rates around roads at Kawamata town after the Fukushima accident. Radiat. Prot. Dosim. 167, 340-343. DOI:10.1093/rpd/ncv275

Malins, A., Okumura, M., Machida, M., Takemiya, H., Saito, K., 2015a. Fields of View of Environmental Radioactivity. In *Proc. Int. Symp. Radiol. Issues Fukushima's Revitalized Futur*. 28-34. Kyoto University Research Reactor Institute.

Malins, A., Okumura, M., Machida, M., Saito, K., 2015b. Topographic effects on ambient dose equivalent rates from radiocesium fallout. In *Proc. M&C + SNA + MC 2015*.

McConn Jr, R.J., Gesh, C.J., Pagh, R.T., Rucker, R.A., Williams III, R.G., 2011. Compendium of Material Composition Data for Radiation Transport Modeling. PNNL-15870 Rev. 1. U.S. Department of Homeland Security. http://www.pnnl.gov/main/publications/external/technical_reports/pnnl-15870rev1.pdf (accessed 20.08.16)

Ministry of Education, Culture, Sports, Science and Technology (MEXT), 2011a. Strengthening of Monitoring in Response to the "Enforced Plan on Environmental Monitoring (May 11, 2011)". http://radioactivity.nsr.go.jp/en/contents/5000/4344/24/1304084_0511.pdf, (accessed 20.08.16)

Ministry of Education, Culture, Sports, Science and Technology (MEXT), 2011b. Distribution map of radiation dose around Fukushima Dai-ichi&Dai-Ni NPP. Nuclear Regulation Authority (NRA), http://radioactivity.nsr.go.jp/en/list/257/list-1.html, (accessed 20.08.16)

Ministry of Education, Culture, Sports, Science and Technology (MEXT) and Nuclear Regulation Authority (NRA), 2012. Monitoring information of environmental radioactivity level, http://radioactivity.nsr.go.jp/en/, (accessed 20.08.16)

Monitoring Coordination Meeting, Japan, 2016. Comprehensive Radiation Monitoring Plan(Revised on 1 April, 2016). Nuclear Regulation Authority (NRA), http://radioactivity.nsr.go.jp/en/contents/12000/11110/24/274%20_20160401.pdf.pdf, (accessed 30.11.16)

Naito, W., Uesaka, M., Yamada, C., Ishii, H., 2015. Evaluation of dose from external irradiation for individuals living in areas affected by the Fukushima Daiichi Nuclear Power Plant accident. Radiat. Prot. Dosim. 163 (3), 353-361. DOI:10.1093/rpd/ncu201

Naito, W., Usesaka, M., Yamada, C., Kurosawa, T., Yasutaka, T., Ishii, H., 2016. Relationship between Individual External Doses, Ambient Dose Rates and Individuals' Activity-Patterns in Affected Areas in Fukushima following the Fukushima Daiichi Nuclear Power Plant Accident. PLoS ONE 11 (8), e0158879. DOI:10.1371/journal.pone.0158879

Nomura, S., Tsubokura, M., Furutani, T., Hayano, R.S., Kami, M., Kanazawa, Y., Oikawa, T., 2016. Dependence of radiation dose on the behavioral patterns among school children: a retrospective analysis 18 to 20 months following the 2011 Fukushima nuclear incident in Japan. J. Radiat. Res. 57 (1), 1-9. DOI:10.1093/jrr/rrv051

Sakamoto, R., Saito, K., 2003. Conversion factors for a mobile survey method by car in the Chernobyl area. Radiat. Prot. Dosim. 106 (2), 165-175.

Sanada, Y., Sugita, T., Nishizawa, Y., Kondo, A., Torii,T., 2014. The aerial radiation monitoring in Japan after the Fukushima Daiichi nuclear power plant accident. Prog. in Nucl. Sci. and Tech. 4, 76-80. DOI:10.15669/pnst.4.76

Sanada,Y., Munakata, M., Mori, A., Ishizaki, A., Shimada, K., Hirouchi, J., Nishizawa,Y., Urabe, Y., Nakanishi, C., Yamada,T., Ishida, M., Sato, Y., Sasaki, M., Hirayama, H., Takamura, Y., Nishihara, K., Imura, M., Miyamoto, K., Iwai, T., Matsunaga, Y., Toyoda, M., Tobita, S., Kudo, T., Nakayama,S., 2016. Radiation Monitoring using Manned Helicopter around the Nuclear Power Station in the Fiscal Year 2015(Contract Research), JAEA-Research 2016-016. (in Japanese), DOI:10.11484/jaea-research-2016-016

Sanada, Y. and Torii,T., 2015. Aerial radiation monitoring around the Fukushima Dai-ichi nuclear power plant using an unmanned helicopter. J. Environ. Radioact. 139, 294-299. DOI:10.1016/j.jenvrad.2014.06.027

Sato, T., Niita, K., Matsuda, N., Hashimoto, S., Iwamoto, Y., Noda, S., Ogawa, T., Iwase, H., Nakashima, H., Fukahori, T., Okumura, K., Kai, T., Chiba, S., Furuta, T., Sihver, L., 2013. Particle and Heavy Ion Transport code System, PHITS, version 2.52. J. Nucl. Sci. Technol. 50(9), 913-923. DOI:10.1080/00223131.2013.814553

Satoh, D., Kojima, K., Oizumi, A., Matsuda, N., Iwamoto, H., Kugo, T., Sakamoto, Y., Endo, A., Okajima, S., 2014. Development of a calculation system for the

estimation of decontamination effects. J. Nucl. Sci. Technol. 51, 656-670. DOI:10.1080/00223131.2014.886534

Tanigaki, M., Okumura, R., Takamiya, K., Sato, N., Yoshino, H., Yoshinaga, H., Kobayashi,Y., 2012. Development of the car-borne survey system KURAMA. Proceedings of PCaPAC2012, Kolkata, India. FRCA03, 248-250. ISBN 978-3-95450-124-3.

Tanigaki, M., Okumura, R., Takamiya, K., Sato, N., Yoshino, H., Yamana, H., 2013. Development of a car-borne γ-ray survey system, KURAMA. Nucl. Instrum. Methods Phys. Res. A 726, 162-168. DOI:10.1016/j.nima.2013.05.059

Torii, T., Sanada, Y., Sugita, T., Kondo, A., Shikaze, Y., Takahashi, M., Ishida, M., Nishizawa, Y., Urabe, Y., 2012. Investigation of Radionuclide Distribution Using Aircraft for Surrounding Environmental Survey from Fukushima Dai-ichi Nuclear Power Plant. JAEA-Technology 2012-036. (in Japanese), DOI:10.11484/jaea-technology-2012-036

Tsuda, S., Yoshida, T., Nakahara, Y., Sato, T., Seki, A., Matsuda, N., Ando, M., Takemiya, H., Tanigaki, M., Takamiya, K., Sato, N., Okumura, R., Kobayashi, Y., Yoshinaga, H., Yoshino, H., Uchihori, Y., Ishikawa, M., Iwaoka, K., Saito, K., 2013. Construction of a Car-borne Survey System for Measurement of Dose Rates in Air: KURAMA-II, and Its Application. JAEA-Technology 2013-037, JAEA. DOI:10.11484/jaea-technology-2013-037. (in Japanese), DOI:10.11484/jaea-technology-2013-037

Tsuda, S., Yoshida, T., Tsutsumi, M., Saito, K., Characteristic and verification of a Car-borne Survey System for Dose rates in Air: KURAMA-II, 2015. J. Environ. Radioact. 139, 260-265. DOI:10.1016/j.jenvrad.2014.02.028

UNSCEAR, 2014. Sources, effects and risks of ionizing radiation, UNSCEAR 2013 report: Levels and Effects of Radiation Exposure Due to the Nuclear Accident after the 2011 Great East-Japan Earthquake and Tsunami. New York, Volume I. http://www.unscear.org/docs/reports/2013/13-85418_Report_2013_Annex_A.pdf

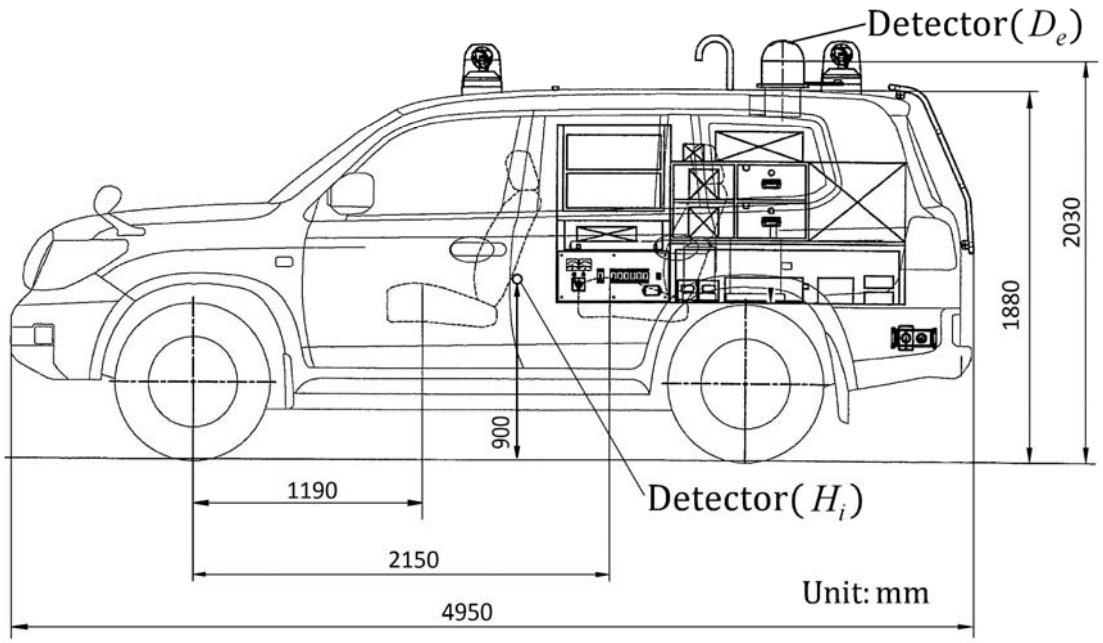

Fig. 1 Specification of JAEA Dedicated Monitoring Vehicle (DMVj).

Vehicle: Toyota CBA-URJ202W. External detectors (D_e) mounted on roof at 2.03 m above the ground include both low range (0.01-10 μGy/h) Hitachi ADP-1122 NaI(Tl) detector and high range (0.01-100 mGy/h) Hitachi ADP-225 SSD detector. The detector installed inside the vehicle (H_i) at 0.9 m above the ground is the Hitachi TCS-172B NaI(Tl) scintillator. Ancillary equipment carried in the rear of the vehicle includes a Pioneer GPS-2003ZZ GPS and a Hitachi ASM-1617 processing unit. The data collection frequency is every 10 s and data are transmitted using NTT DOCOMO FOMA communication systems.

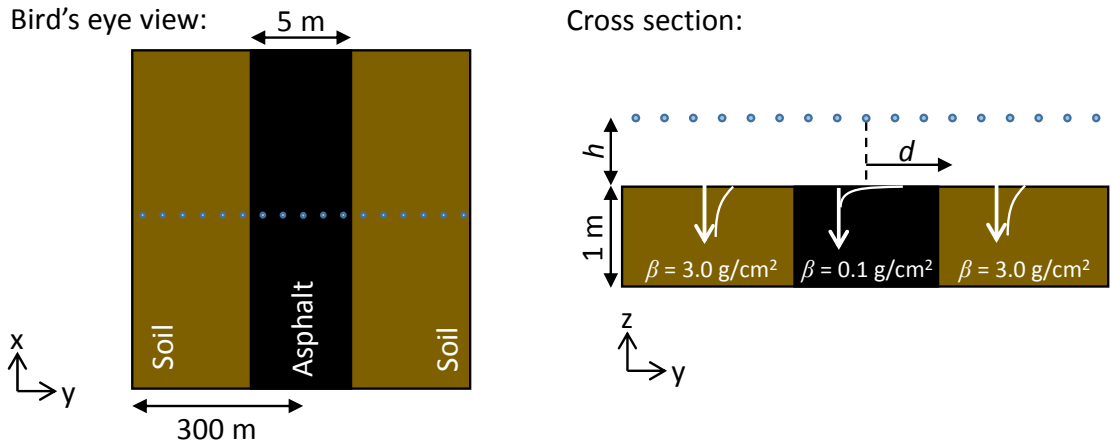

Fig. 2 Diagram of the Monte Carlo calculation for the $H^*(10)$ distribution across a model road. Ambient dose equivalent rates are calculated at heights h = 0.5, 1, 2 & 3 m above the road, for distances d = 0, 1, 2, 3 m… from the center of the road. The inset graphs in the right hand panel show the exponential depth distributions of ^{134}Cs and ^{137}Cs in the soil and asphalt media.

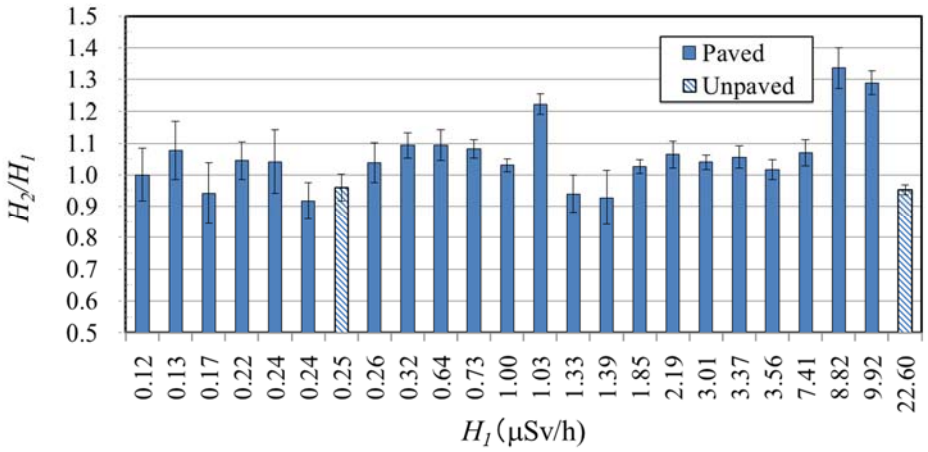

Fig. 3 Ratio of ambient dose equivalent rates measured with the hand-held survey meter at 2 and 1 m heights (H_2/H_1), as a function of ascending H_1. Error bars show ± one standard deviation uncertainty about the mean over the five measurement directions.

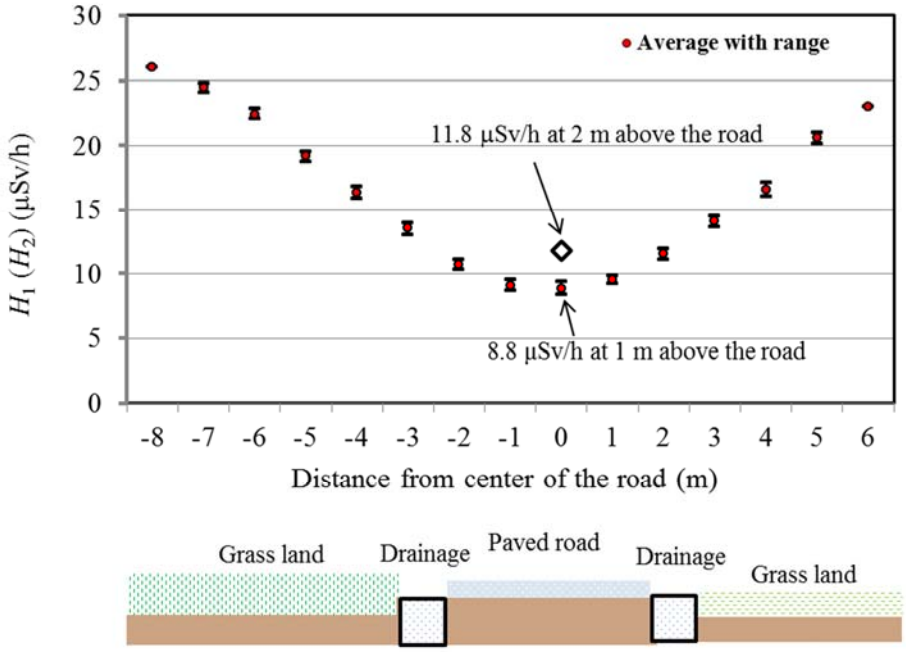

Fig. 4 Distribution of ambient dose equivalent rates perpendicular to the road at calibration site O-6.

(a)

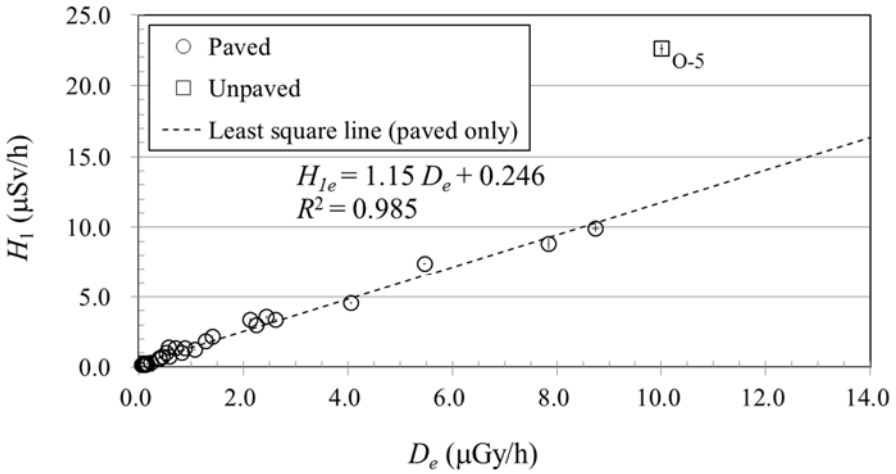

(b)

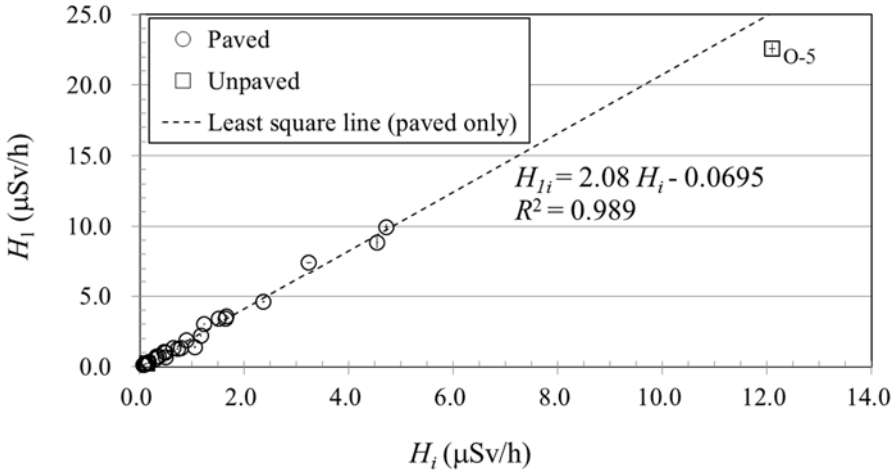

Fig. 5 Scatter plot of H_1 against (a) D_e and (b) H_i measured at 29 paved calibration sites. Dotted lines are linear least squares best fits, yielding parameters a_{1e}, b_{1e} (panel (a)) and a_{1i}, b_{1i} (panel (b)).

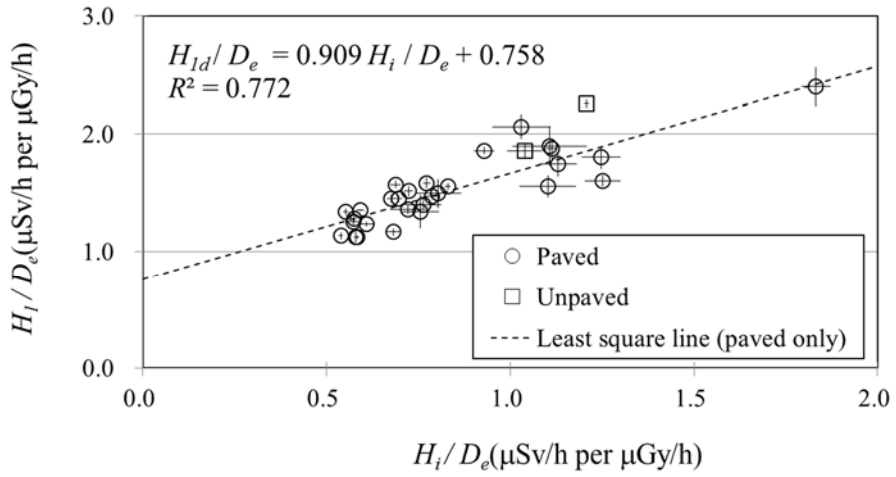

Fig. 6 Scatter plot of H_1/D_e against H_i/D_e used to determine parameters a_{1d} and b_{1d} for the dual-detector setup.

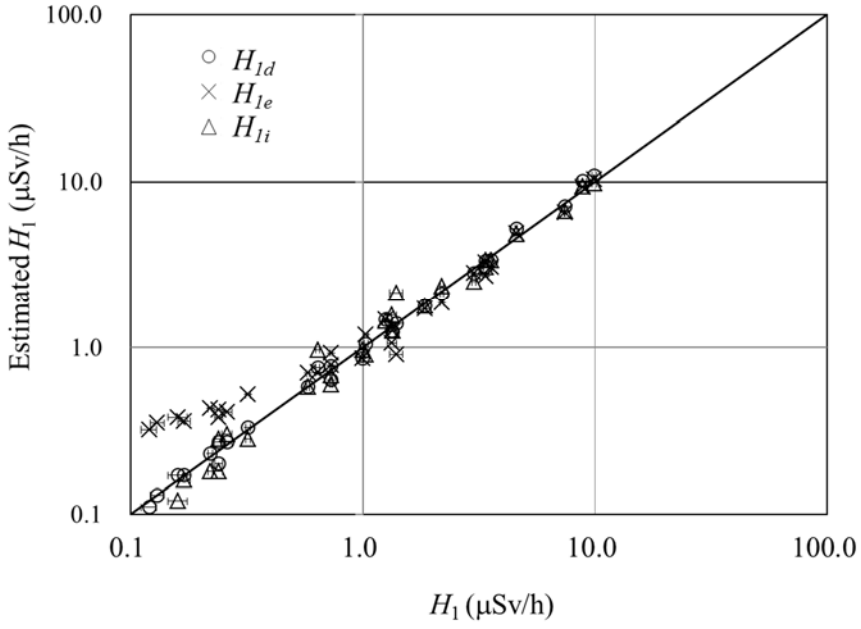

Fig. 7 Correlation of converted ambient dose equivalent rates using the single detectors (H_{1e} and H_{1i}) and the dual-detector (H_{1d}) against H_1.

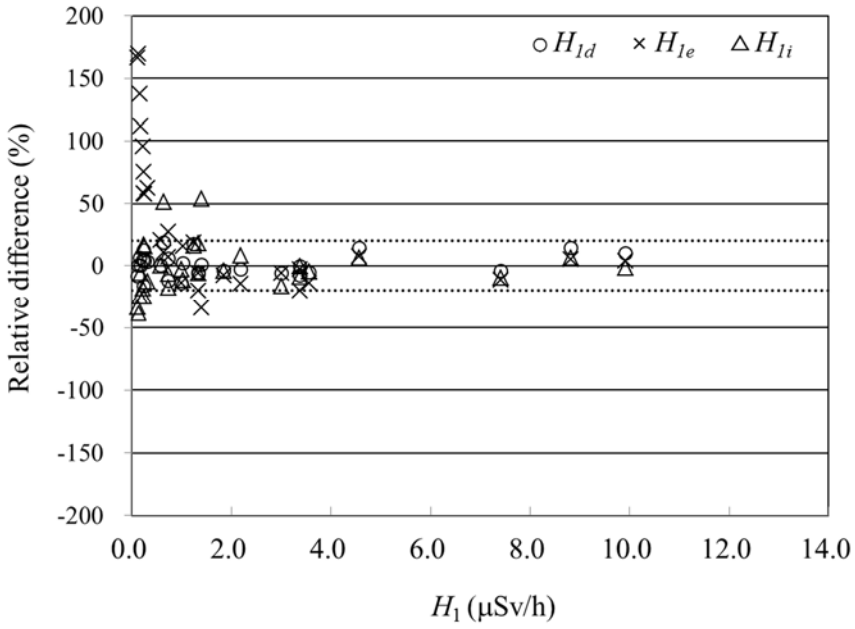

Fig. 8 Relative differences between the DMVj converted results and the reference hand-held measurements H_1, as a function of increasing H_1. Dotted lines indicate ±20% relative difference.

(a)

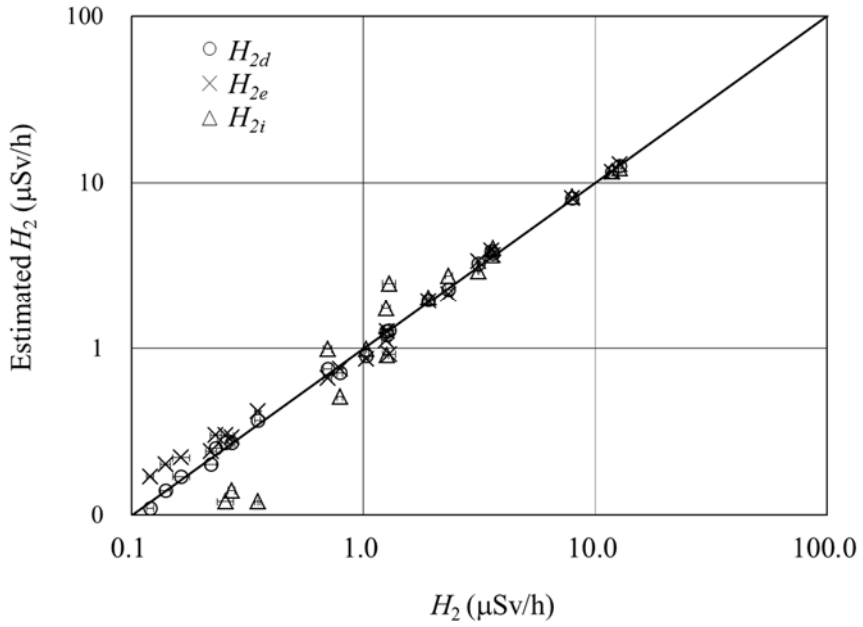

(b)

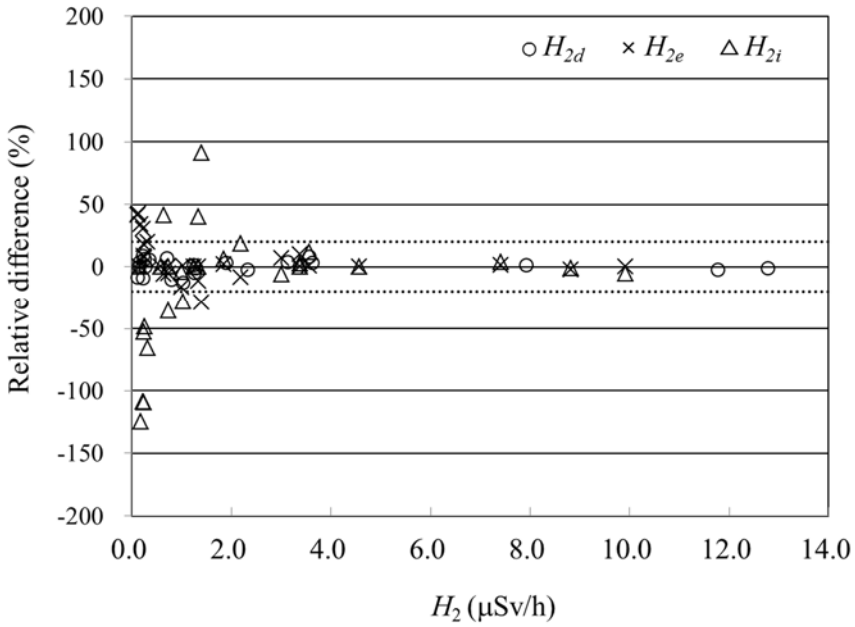

Fig. 9 Ambient dose equivalent rate estimates at 2 m. (a) Correlation between DMVj estimates and the reference H_2 values. (b) Relative differences between DMVj estimates and the reference H_2 values. Dotted lines indicate ±20% relative difference.

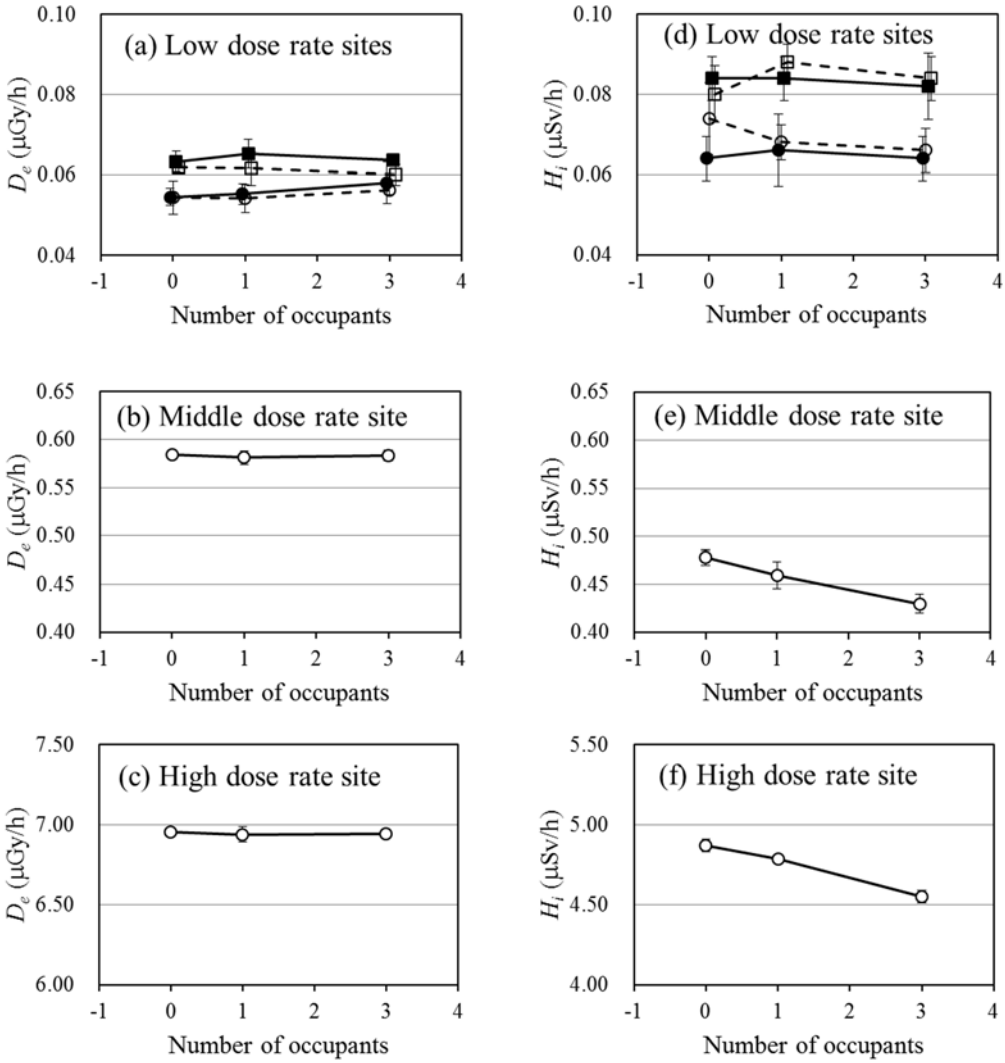

Fig. 10 Effect of vehicle occupant number on responses of the DMVj external (panels (a) to (c)) and internal detector ((d) to (f)). Data are shown for two separate sites in panels (a) and (d), as distinguished by square and circle markers. The solid marks and lines in panels (a) and (d) are for measurements at the beginning of the 135 km round-trip journey (i.e. full fuel tank), while the open marks and dashed lines are measurements at the end of the trip when one quarter of the fuel had been burned.

(a)

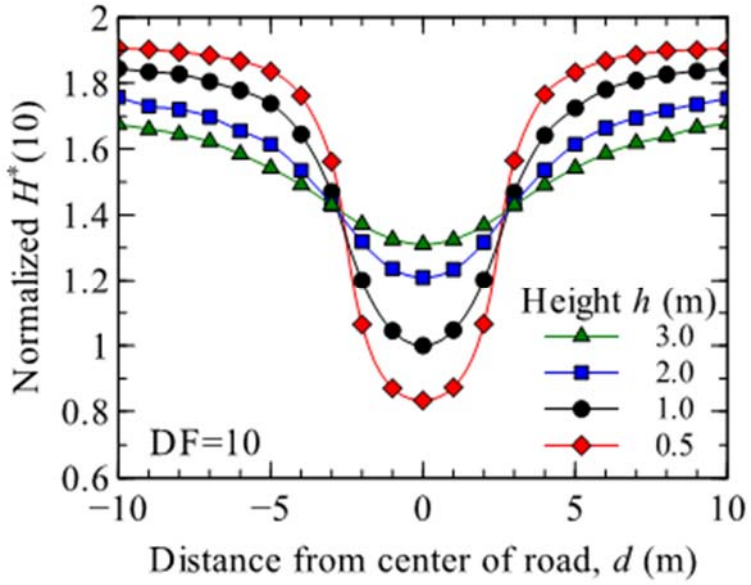

(b)

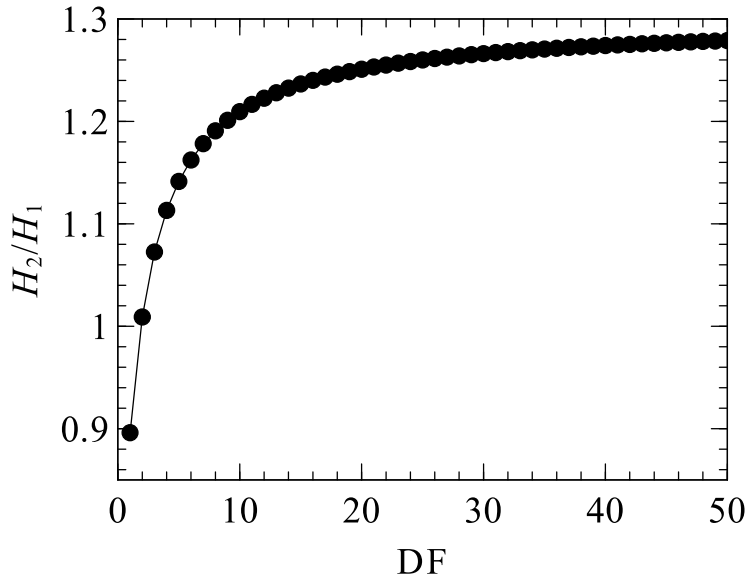

Fig. 11 (a) Results of Monte Carlo simulation of the ambient dose equivalent rate distribution perpendicularly across a 5 m road and adjacent land. Different lines indicate height above ground surface. The ambient dose equivalent rates are normalized by $H^*(10)$ at 1 m above the center of the road. (b) Ratio H_2/H_1 at center of road as a function of the decontamination factor (DF) of radiocesium from the road compared to adjacent land.

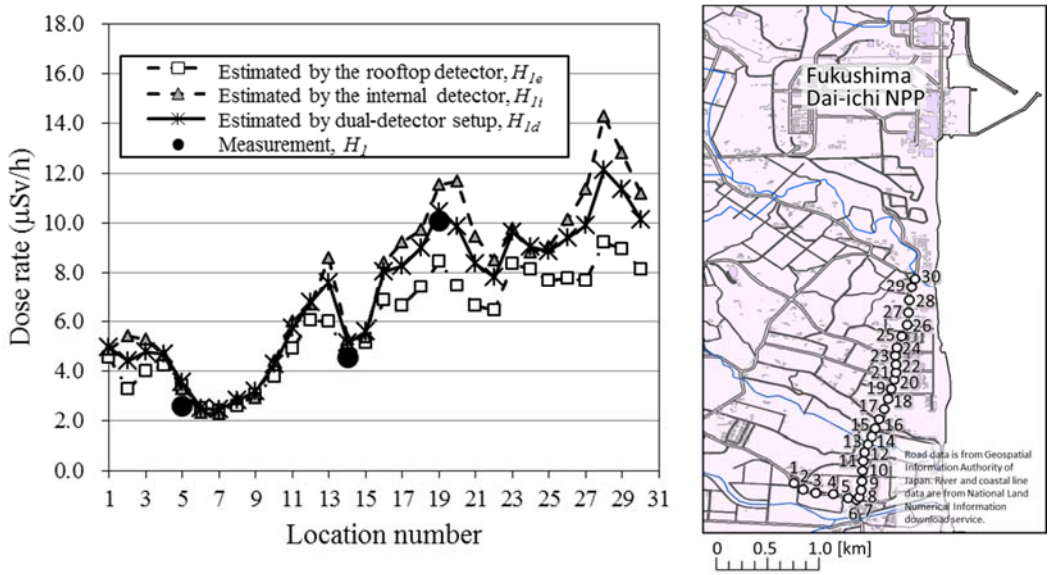

Fig. 12 Ambient dose equivalent rates estimated by the DMVj individual detectors and the dual-detector setup when driven through the Okuma area between 1.8 and 4 km south of the FDNPP site. Location numbers are shown in the right hand panel.

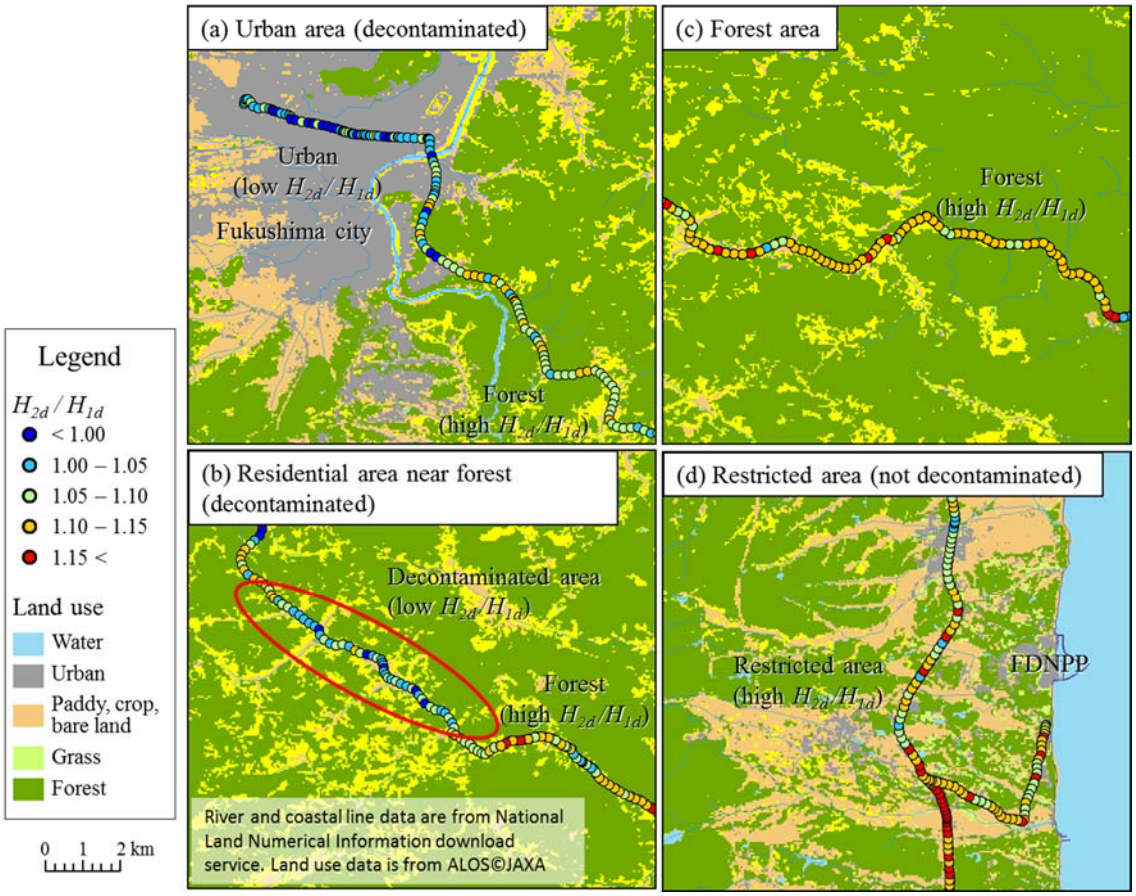

Fig. 13 Ratio of ambient dose equivalent rates at 1 and 2 m height estimated by dual-detector setup in an urban area (a), a residential area near forest (b), a forest area (c) and a restricted area (d). The ratio H_{2d}/H_{1d} tends to be low in urban, residential and decontaminated areas, while it tends to be high in forest areas and restricted areas that are not decontaminated.

Table 1 Measured and calculated quantities, their symbols and units.

Symbol	Unit	Description
		Measured quantities
D_e	μGy/h	Absorbed dose rate in air (from DMVj external detector ~2.0 m)
H_i	μSv/h	$H^*(10)$ inside vehicle (from DMVj internal detector ~0.9 m)
H_1	μSv/h	$H^*(10)$ measured at 1 m with hand-held detector without DMVj
H_2	μSv/h	$H^*(10)$ measured at 2 m with hand-held detector without DMVj
		Calculated quantities[†]
H_{xe}	μSv/h	$H^*(10)$ at x m without DMVj derived from D_e alone
a_{xe}	μSv/μGy	Conversion coefficient #1 for D_e to H_{xe}
b_{xe}	μSv/h	Conversion coefficient #2 for D_e to H_{xe}
H_{xi}	μSv/h	$H^*(10)$ at x m without DMVj derived from H_i alone
a_{xi}	-	Conversion coefficient #1 for H_i to H_{xi}
b_{xi}	μSv/h	Conversion coefficient #2 for H_i to H_{xi}
H_{xd}	μSv/h	$H^*(10)$ at x m without DMVj derived from D_e and H_i (dual-detector setup)
a_{xd}	-	Conversion coefficient #1 for dual-detector setup to H_{xd}
b_{xd}	μSv/μGy	Conversion coefficient #2 for dual-detector setup to H_{xd}

[†] x denotes 1 or 2 m height above surface

Table 2 Measurement results from calibration sites. Direction and distance columns indicate location of calibration site with respect to the FDNPP site.

Location								
Date (day/month /year)	ID	Direction	Distance (km)	Surface*	H_1 (μSv/h)	H_2 (μSv/h)	D_e (μGy/h)	H_i (μSv/h)
19/03/2015	A-1	WNW	30	R	1.33 ± 0.06	1.25 ± 0.05	0.71 ± 0.005	0.79 ± 0.008
19/03/2015	79	WNW	29	PL	2.19 ± 0.04	2.33 ± 0.08	1.41 ± 0.005	1.17 ± 0.008
19/03/2015	A-10	WNW	26	PL	3.01 ± 0.06	3.13 ± 0.03	2.25 ± 0.007	1.24 ± 0.013
19/03/2015	O-1	WSW	5.0	PL	3.56 ± 0.08	3.62 ± 0.08	2.45 ± 0.009	1.66 ± 0.026
19/03/2015	Ot-1	S	1.5	R	9.92 ± 0.25	12.8 ± 0.19	8.75 ± 0.057	4.72 ± 0.030
18/08/2015	78	NW	48	PL	0.24 ± 0.01	0.22 ± 0.01	0.12 ± 0.004	0.12 ± 0.008
18/08/2015	i-8	NW	44	BL	0.25 ± 0.01	0.24 ± 0.01	0.13 ± 0.003	0.14 ± 0.005
18/08/2015	i-6	NW	41	SR	0.64 ± 0.01	0.70 ± 0.03	0.40 ± 0.009	0.50 ± 0.016
18/08/2015	i-7	NW	42	R	0.73 ± 0.01	0.79 ± 0.02	0.46 ± 0.007	0.32 ± 0.004
18/08/2015	i-23	NW	35	R	1.00 ± 0.01	1.03 ± 0.02	0.54 ± 0.008	0.50 ± 0.012
20/08/2015	O-2	WSW	4.8	PL	1.03 ± 0.02	1.26 ± 0.02	0.82 ± 0.008	0.47 ± 0.012
20/08/2015	O-3	WSW	4.9	PL	3.37 ± 0.07	3.56 ± 0.09	2.63 ± 0.013	1.51 ± 0.015
20/08/2015	O-4	S	1.6	PL	7.41 ± 0.03	7.93 ± 0.31	5.47 ± 0.017	3.24 ± 0.053
20/08/2015	O-5	S	1.4	BL	22.6 ± 0.34	21.5 ± 0.13	10.0 ± 0.029	12.1 ± 0.055
21/08/2015	20	WNW	41	R	0.12 ± 0.01	0.12 ± 0.004	0.06 ± 0.003	0.07 ± 0.005
21/08/2015	10	WNW	44	SR	0.13 ± 0.01	0.14 ± 0.01	0.09 ± 0.004	0.07 ± 0.004
21/08/2015	42	W	30	SR	0.16 ± 0.02		0.12 ± 0.006	0.09 ± 0.004
21/08/2015	23	WNW	37	R	0.17 ± 0.01	0.16 ± 0.01	0.10 ± 0.002	0.11 ± 0.004
21/08/2015	41	W	20	SR	0.22 ± 0.00	0.23 ± 0.01	0.16 ± 0.003	0.12 ± 0.007
21/08/2015	113	W	25	R	0.24 ± 0.01	0.25 ± 0.02	0.15 ± 0.006	0.17 ± 0.010
13/10/2015	i-4	NW	41	R	1.39 ± 0.09	1.29 ± 0.08	0.58 ± 0.010	1.06 ± 0.011
14/12/2015	F-5	NNW	3.5	SS	0.58 ± 0.01		0.39 ± 0.002	0.31 ± 0.007
14/12/2015	F-4	NNW	4.4	R	0.73 ± 0.01		0.59 ± 0.008	0.36 ± 0.013
14/12/2015	F-1	NW	3.0	SR	1.25 ± 0.03		1.07 ± 0.010	0.73 ± 0.022
14/12/2015	F-2	NNW	4.0	PL	1.34 ± 0.04		0.88 ± 0.005	0.64 ± 0.010
14/12/2015	F-6	NNW	4.1	R	3.38 ± 0.09		2.13 ± 0.008	1.65 ± 0.021
14/12/2015	F-3	NNW	3.9	R	4.57 ± 0.05		4.06 ± 0.010	2.37 ± 0.023
09/02/2016	Nr-2	S	15	R	0.26 ± 0.01	0.27 ± 0.01	0.14 ± 0.002	0.18 ± 0.007
09/02/2016	Nr-1	SSW	13	SR	0.32 ± 0.01	0.35 ± 0.01	0.24 ± 0.002	0.17 ± 0.011
09/02/2016	N-1	NW	26	PL	1.85 ± 0.03	1.90 ± 0.03	1.28 ± 0.007	0.89 ± 0.008
09/02/2016	O-6	S	1.4	R	8.82 ± 0.38	11.78 ± 0.24	7.84 ± 0.006	4.54 ± 0.020

* R, paved Road; PL, Paved parking Lot; SR, Side of the Road; BL, Bare Land without pavement; SS, paved Stopping Space in front of a building